NTNU – Trondheim
Norwegian University of
Science and Technology

An Imaging Spectrometer using an Acousto-Optic Tunable Filter

Andre Tor Rikard Ingvaldsen

Master of Science in Engineering Cybernetics
Submission date: June 2012
Supervisor: Amund Skavhaug, ITK

Norwegian University of Science and Technology
Department of Engineering Cybernetics

Preface

This report is the result of my master thesis project carried out in my final semester of the Master's programme in Engineering Cybernetics at the Norwegian University of Science and Technology. It is a continuation of the work I did in the preliminary project the previous semester. The assignment was given after prof. Bjørn Alsberg of the Department of Chemistry came to our department and asked for help to construct a hyperspectral imaging system.

The system design is based on a scientific digital camera that had been acquired for a similar project that was never finished. Therefore, there was no available work to build on and we started from scratch to design the system. In the preliminary project a suitable acoust-optic tunable filter was chosen to be the wavelength selective element. The design presented in this report is based on these two components. The intention was to construct a prototype of the system, but due to technical difficulties this has not been possible. We sent a defective part for repair early on, but it was never returned. Instead we present how the system would be built and what and experiments was planned.

I would like to thank my supervisor, Amund Skavhaug, for the support he has given me throughout my project. I would also like to thank Lise Randeberg at the Department of Electronics and Telecommunications for giving me helpful pointers in my work. Credits is given to my friend Anders Hoff for helping out with figures and LaTeX, and for helpful discussions about the project.

André Ingvaldsen

June 05, 2012

The major difference between a thing that might go wrong and a thing that cannot possibly go wrong is that when a thing that cannot possibly go wrong goes wrong it usually turns out to be impossible to get at or repair.

– Douglas Adams, Mostly Harmless

Abstract

Spectroscopy is a powerful tool for analysis in a wide range of scientific and industrial fields. Spectroscopic measurements obtain information about the interaction between matter and radiated energy. This information may be utilized for detection and classification of objects and substances. There is a wealth of different methods and technologies developed for different applications, from space- and air-borne remote sensing to medical sample analysis.

In this report we present a spectral imaging system consisting of a digital camera with an acousto-optical tunable filter (AOTF) as the spectral band selective element. An evaluation of the properties of the imager is presented, and we investigate the feasibility of real-time spectral imaging video based on this system. A comparison with other spectral imaging technologies is made. Custom application software for camera control and image acquisition is presented. A special optical layout that minimizes the optical aberrations produced by the diffraction process in the AOTF is also presented.

The system produce a stack of monochrome images at different wavelength bands forming an "image cube" containing a combination of spatial an spectral information. The system uses the visible part of the electromagnetic spectrum to collect spectral information at every point in an image plane. Our results show that the camera have good light sensitivity and a high signal-to-noise ratio, but that the image throughput and spatial resolution is not optimal for a high image rate. The AOTF is a highly flexible device with random access to wavelength bands and selectable band-pass shape. But the many configurable parameters of the system also complicates usage. Many parameters need to be calibrated, and we present some methods on this. A major challenge in an spectral imaging system is to get enough light through to the sensor, and we find that there is high loss of light caused by the diffraction process in the filter. It will be shown that the system is not suitable for real-time spectral video imaging because of the low frame rate. Suggestions for improvements are given.

Sammendrag

Spektroskopi et nyttig analyseverktøy i et bredt spekter av vitenskapelige og industrielle felt. Spektroskopiske målinger henter inn informasjon om samspillet mellom materie og utstrålt energi. Denne informasjonen kan brukes for å detektere og klassifisere gjenstander og stoffer. Det finnes et vell av ulike metoder og teknologier som er utviklet for ulike bruksområder, fra overvåkning av jordoverflaten fra luften eller verdensrommet, til medisinsk analyse av prøver.

I denne rapporten presenterer vi et spektralt avbildningssystem bestående av et digitalkamera med et akusto-optisk tunbart filter (AOTF) for å skille ut spektralbåndene. Vi evaluerer egenskapene til systemet og undersøker muligheten for spektral avbildning med sanntidsvideo basert på dette systemet. En sammenligning med andre teknologier for spektral avbildning har blitt utført. Spesialutviklet programvare for kamerakontroll og bildetaking er presentert. Et spesiellt optisk oppsett som minimerer optiske aberrasjoner produsert av diffraksjonsprosessen i AOTF-en er også presentert.

Systemet produserer en stabel med monokromatiske bilder i ulike bølgelengdebånd som danner en "bildekube" som inneholder en kombinasjon av romlig en spektral informasjon. Systemet bruker den synlige delen av det elektromagnetiske spekteret til å samle spektral informasjon på hvert punkt i et bildeplan. Våre resultater viser at kameraet har god lysfølsomhet og et høyt signal-til-støy-forhold, men at bildegjennomstrømming og romlig oppløsning ikke er optimal for en høy bildehastighet. AOTF-en er en svært fleksibel enhet med direkte tilgang til bølgelengdebånd og valgbar båndpassform. Men de mange konfigurerbare parameterne i systemet kompliserer også bruken. Mange parametere må kalibreres, og vi presentere noen metoder på dette. En stor utfordring i et spektralt avbildningssystem er å få nok lys gjennom til sensoren, og det viser seg at mye lys går tapt på grunn av diffraksjonsprosessen i filteret. Vi konkluderer med at systemet ikke er egnet for spektral video i sanntid på grunn av for lav bildefrekvens. Forslag til forbedringer blir gitt.

Contents

Preface **i**

Abstract **v**

Sammendrag **vii**

List of Figures **1**

List of Tables **2**

1 Introduction **3**

1.1 Related work 4

1.2 Report outline 5

2 Background Theory **7**

2.1 Imaging spectroscopy 7

2.1.1 Spectral reflectance 8

2.2 Hyperspectral imaging 8

2.2.1 Sensor technology 9

2.2.2 Spectral classification and detection 11

2.3 EMCCD camera 12

2.3.1 Electron multiplication 12

2.3.2 Quantum efficiency 12

2.3.3 Frame transfer CCD 13

2.3.4 Acquisition modes 16

2.3.5 Frame rate and binning 17

2.4 Acousto-optical tunable filter (AOTF) 18

2.5 Radio frequency driver 22

2.6 Optics 23

2.6.1 Telecentricity 23

2.7 LabVIEW 24

2.7.1 Dataflow programming 25

2.7.2 The G programming language 25

3 AOTF-based spectral imaging system 27

3.1 Camera specifications 27
3.2 AOTF specifications 27
3.3 RF driver setup 30
3.4 Optical configuration 30
3.5 Application 32
3.6 Calibration 32
3.6.1 Radiometric calibration 33
3.6.2 Spectral calibration 33
3.6.3 Geometric calibration 34
3.6.4 Noise calibration 34

4 Assembly and testing 37

4.1 Alignment of optics 37
4.2 Synchronization 39

5 Discussion 41

5.1 Quality of the design 41
5.2 Implications 42
5.3 Suggestions 44

6 Conclusion 45

Appendices

Appendix A LabVIEW diagrams 51

List of Figures

1 Multispectral/hyperspectral imaging comparison 9
2 Quantum efficiency 13
3 Frame transfer CCD 14
4 Capture sequence for a frame transfer CCD 15
5 Kinetic Series mode 17
6 AOTF operating priciples 20
7 Combination of different spectral bands 22
8 System overview 27
9 AOTF specifications 29
10 Optical layout 31
11 Lens position 39
12 Top level VI 52
13 Set parameters VI 54
14 Acquire multicore VI 56
15 Acquire singlecore VI 58
16 Temperature control VI 60
17 Calculate FPS VI 61
18 Camera error handler VI 63
19 Shutdown camera VI 64

List of Tables

1 Camera frame rates 18
2 Ideal tunable filter attributes 19
3 EMCCD camera specifications 28
4 AOTF specifications 28
5 System parameters 37
6 Spectral bands used during testing. 40
7 Image cube acquisition times 43

1 Introduction

Spectroscopy is the study of how radiated energy and matter interact. By measuring how radiation intensity varies over a wavelength region, inference can be made about the composition of the matter. Although many types of radiated energy may be used for spectroscopic measurements, the most widely used is the different parts of the electromagnetic spectrum. Different methods are classified by the wavelength region of the spectrum used. Imaging spectroscopy is a branch of spectroscopy that is related to color photography, in which spectral information is combined with spatial information. The measurements data forms stack of monochrome images taken at different wavelengths, known as an "image cube". The number of image planes making up the image cube varies. When many narrow contiguous spectral bands are captured, the spectral image may be thougth of as having full spectra at every location in the image. This is commonly known as hyperspectral imaging. The alternative is known as multispectral imaging, when the spectral bands are fewer and not forming the full spectrum.

Imaging spectroscopy techniques are finding use in medicine, agriculture, manufacturing, forensics, and many other applications [1–4]. Various spectral imaging techologies that acquire the spectral data in different manners have been developed. Line scanning systems, called push-broom imagers, capture one spatial dimension and the full spectral dimension at a time, scanning over the scene to capture the second spatial dimension. Such systems use a diffraction grating or prisms to split the incident light into its wavelength components. On the other hand there is tunable filter systems that work in a band-sequential manner, capturing a full spatial image at each spectral band and capturing the spectral dimension displaced in time [5]. There are several filter technologies to choose from, from filter wheels that are manually operated to various electronically tunable band-pass filter types. Push-broom imagers seems a natural choice when the system is moving in one dimension relative to the scene that is being imaged. One example of this is the field of remote sensing, in which earth resources is being monitored from the air or from space [6]. By

the same reasoning band-sequential imagers are a natural choice for stationary applications. However, both types of hyperspectral imaging systems can be used in both mobile and stationary settings.

The purpose of this study is to design a band-sequential hyperspectral imaging system that uses an acousto-optic tunable filter (AOTF) to select the spectral bands. A scientific grade digital camera is used to capture the images. We find out and evaluate the system parameters, including spatial and spectral resolution, framerate, optical characteristics and light collection efficiency. As the system is meant to be a step towards a system able to deliver real-time spectral video, we investigate the potential for real-time operation. We present an optical layout that is made to conform to the characteristics of the AOTF. The work presented in this report is a continuation of the preliminary project that were done by the author and parts of this report is based on the report produced for that project. In the previous project the camera properties was examined and the camera–filter synchronization issue was solved. This report takes system integration perspective, and does not explore processing of spectral data in-depth.

1.1 Related work

There are some noteable related work on spectral imaging systems using AOTFs. Vila-Francés et al. [7, 8] has implemented a spectral imaging system based on an AOTF and present an optical layout that our design is based on. A treatment on optics for aberration correction of acousto-optic tunable filters is given in Suhre et al. [9]. Hyperspectral imaging systems based on AOTFs have been implemented by Gupta [10] and Farries et al. [11]. Gat [5] gives a review of tunable filter technology, and give advice on system integration. Geladi et al. [12] presents some concepts in calibration of spectral imaging systems, and signal treatment. Liu et al. [13] presents some specific calibration setups and methods on AOTF hyperspectral imagers.

1.2 Report outline

In the first part of this report we review the relevant background theory. First we introduce the principles in imaging spectroscopy in general and more specifically hyperspspectral imaging. We go on to review the working principles and properties of the camera used in this project and acousto-optical tunable filters. Then we present some optical concepts relevant to this system. Lastly, we give an introduction to the LabVIEW software package. In the second part the design of the spectral imaging system is presented, and some calibration methods are presented. In the last part of this report we go through assembly and initial testing of the system, followed by discussion and conclusion.

2 Background Theory

In this section we explore some background theory, and describe the functions of the components that makes up the spectral imaging system. First, we have a look at imaging spectrocopy, and go more into more detail on hyperspectral imaging. We then go through the properties of the camera, and review the filter technology. The next part explore some of the relevant theory on optics. Finally, an introduction to the software platform LabVIEW from National Instruments is given.

2.1 Imaging spectroscopy

Imaging spectroscopy is a term used to describe a set of techniques that collects light intensity data from several spectral bands. The term is sometimes used interchangeably with hyperspectral imaging, but is collective term for a family of imaging methods (i.e. hyperspectral, multispectral, and chemical imaging).

In color photography each pixel contains spectral information in three bands; red, green, and blue. Imaging spectroscopy is similar to color photography, but with each pixel made up of many bands of light intensity data (refer to Figure 1). These spectral data are utilized to derive information about matter based on the signature of the interaction of light and matter expressed in the spectrum.

Every material — solid, gas, or liquid — is formed by chemical bonds and can potentially be detected by spectroscopy. Actual detection depend on the spectral coverage, spectral resolution, and signal-to-noise ratio of the spectrometer, as well as other factors like the abundance of the material in the scene and the strength of absorption/reflectance features for the material in the wavelength region measured.

Several factors influence the sensed spectra depending on the environment of the spectrometer. To be able to extract useful information about the scene we need to know the emission spectrum of the light source. The solar emission spectrum

is well known, but if daylight is used as the source of illumination factors such as atmospheric absorption, scattering and emission will influence the sensed spectra. These factors are variable and difficult to correct for in the spectrometer. If the spectrometer is to be used indoors a light source with a known emission spectrum can be used and the spectrometer calibrated accordingly. In either case local effects such as shadowing will affect the acquired spectra. Such effects are generally unknown, making them hard to correct.

2.1.1 Spectral reflectance

In reflected light spectroscopy the information we want to obtain is *spectral reflectance*: the proportion of reflected light versus incident light as a funtion of wavelength. For most materials reflectance varies with wavelength because light at certain wavelengths is scattered or absorbed to different degrees [6]. When a material is irradiated several physical processes take place that determine the nature of the reflected light. First, some light rebounds directly from the surface of the material in a similar way to a mirror, known as specular reflection. The spectrum of the reflected light remains the same as the incident light. Second, some light diffuses into the material where some is absorbed and some is scattered randomly from the internal pigment of the material. This is known as diffuse reflection [14].

2.2 Hyperspectral imaging

Hyperspectral imaging (HSI) collects and process data from across a contiguous part of the electromagnetic spectrum. The spectral image data is made up of a stack of hundreds of images, each image aquired at a narrow spectral band, thus forming a data cube of two spatial and one spectral dimension. In Figure 1 a comparison of multispectral and hyperspectral imaging is shown. Each image cell in the hyperspectral image represents the continuous spectrum at that point in the scene. In mutispectral imaging the spectrum is also divided into somewhat narrow bands, but unlike hyperspectral imaging the continuous spectrum is not

produced, as illustrated in Figure 1. The spectral bands are typically fewer and wider than in hyperspectral imaging, and not contiguous parts of the spectrum [6, 15].

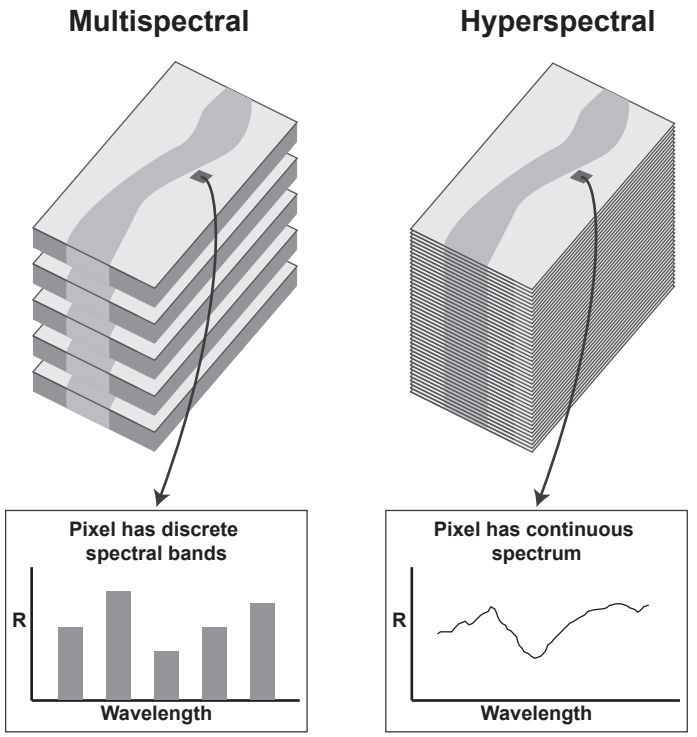

Figure 1: Multispectral and hyperspectral imaging comparison. The datacubes are formed by a stack monochrome images in different spectral bands.

2.2.1 Sensor technology

Several HSI technologies have emerged over time, from the remote sensing technology developed for Earth resource monitoring by NASA to applicatons in medicine, agriculture, mineralogy, manufacuring, forensics and many others [1, 3, 4]. The different technologies can be divided into three groups — push-

broom sensors, tunable filter sensors and 4D sensors — which are introduced below.

In remote sensing and other mobile applications a line scanning process is often applied, commonly known as push-broom imaging. Push-broom imagers acquire one line image at the time in a way that the full spectral data is collected for each pixel in the line simultaneously. Usually a diffraction grating is used, diffracting the light into its wavelength components and projecting it onto a 2D array detector. The full hyperspectral image is built line by line. When imaging a sample with push-broom system, either the sample or the imager need to move or be moved. Push-broom HSI is a natural choice when there are a one-dimensional movement between the sensor and the object, such as in air- or space-borne remote sensing, or optical inspection over a conveyor belt [6, 15].

Tunable filter imagers acquire the two spatial dimensions in each frame, while the spectral dimension is captured over a period of time. This can be accomplished by swapping narrow band pass filters in front of a monochrome camera. Using electronically tunable filters (ETF) to achieve the same effect is a solution that will allow for higher image rates and a more flexible system [5, 11]. A variety of ETF types have been used in imaging modes, the main categories being liquid crystal devices based on birefringence, acousto-optic devices based on diffraction and interferometer types like Fabry-Perot and fourier transform spectrometers [5]. A tunable filter imager seems an evident choice for imaging in stationary applications. With high speed cameras becoming more available and filter technology maturing, sequential hyperspectral imagers are becoming more prevalent [2, 10].

Lastly, there have been developed imaging spectrometers that can capture a full image cube in a single exposure. These systems sacrifice spatial resolution, but in return have high spectral and temporal resolution. Such instruments are ideal for capturing events that are changing very rapidly. Example applications include lightning characterization, missile plume phenomenology and gas gun impact tests [16].

2.2.2 Spectral classification and detection

The relevant applications of this system are related to target detection and classification rather than pattern classification as commonly considered in remote sensing literature. In pattern classification a classifier must classify image data into a number of pattern classes, including background classes. Because image background varies and are difficult to characterize and because many unknown signal sources may be present in the image data, it is nearly impossible to classify image background without complete prior knowlegde. On the other hand, in target classification we are generally interested in classification of targets rather than image background. In many situations, we may have prior knowlegde about targets we want to classify. Moreover, we can obtain such knowledge beforehand if we are searching for a specific material. We may then perform target classification without need for background knowledge.

Automatic processing of conventional images is hampered by the ambiguity inherent in 2D images of 3D scenes. Spectral information greatly facilitates automatic processing. Pixel spectra are multivariate data and can be considered points in a space with dimensions equal to the number of bands. High dimensionality gives less ambiguity and greater separation. The challenge is to find rules for classification or detection of data. Using the taxonomy of Chang [15], we make a distinction among detection, classification, discrimination, identification and quantification. To clarify, target detection does not necessarily imply target classification, neither does target classification imply target discrimination. A target detector which achieves 100% detection may result in 0% classification since it may not be able to classify the detected targets. One such detector is an anomaly detector, which searches for extraordinary pixel spectra, but may not be able to classify the detected anomalies. Similarly, a target classifier may classify targets correctly, but may fail to discriminate all the classified targets. On the other hand, a target discriminator may discern one target from another, but does not necessarily classify these targets. A target identifier usually requires a database or spectral library to identify targets of interest. It performs more subtle funtionality than detection, classification and discrimination [15].

2.3 EMCCD camera

In this section we describe some aspects of the digital camera used in this project. The camera is a scientific digital camera with an electron multiplying charge coupled device (EMCCD). The EMCCD allows for high sensitivity at high frame rates without increasing the readout noise noticeably. In addition, the camera incorporates cooling of the sensor head. Cooling reduce noise by lowering the dark current reducing the effect of blemishes in the sensor.

2.3.1 Electron multiplication

Traditional CCD sensors offers high sensitivity at the expense of slow readout. The constraint is due to the CCD charge amplifier. To achieve high speed operation the bandwidth of the charge amplifier needs to be as wide as possible, but noise scales with the bandwidth of the amplifier. Hence higher speed amplifiers have higher noise levels. This is why ordinary CCDs use relatively low bandwidth and, as a result, relatively modest readout speeds. EMCCD sensors avoid this constraint by amplifying the charge signal before the charge amplifier, maintaining good sensitivity at high speeds. By amplifying the signal in this way the readout noise is effectively bypassed and no longer limiting the sensitivity. An illustration of the CCD is provided in Figure 3. It shows the multiplication register where electron multiplication takes place, before the on-chip charge-to-voltage conversion.

2.3.2 Quantum efficiency

Quantum efficiency (QE) is a measure of the of the effectiveness of an imager to produce electronic charge from incident photons. QE is often given in percentage of photons hitting the sensor surface that will produce a charge. Since the energy of a photon is inversely proportional to its wavelength QE varies over the wavelength range of the imager. Ordinary CCDs typically have QE curves

that are low in the blue segment of the visible spectrum and peaks in the red or near infrared region.

This camera has a back-illuminated and thinned CCD making it more sensitive compared to ordinary CCDs. The thickness of the sensor is uniformy reduced so that an image can be focused on the back of the array where there is no gate structure. Since light is hitting the silicon directly instead of passing through the gate structure, sensitivity to blue light is particularly good [5]. The QE curve of the camera is shown in Figure 2. The QE lies above 70% throughout the effective wavelenght interval of the AOTF used in the system, which is 450–800 nm.

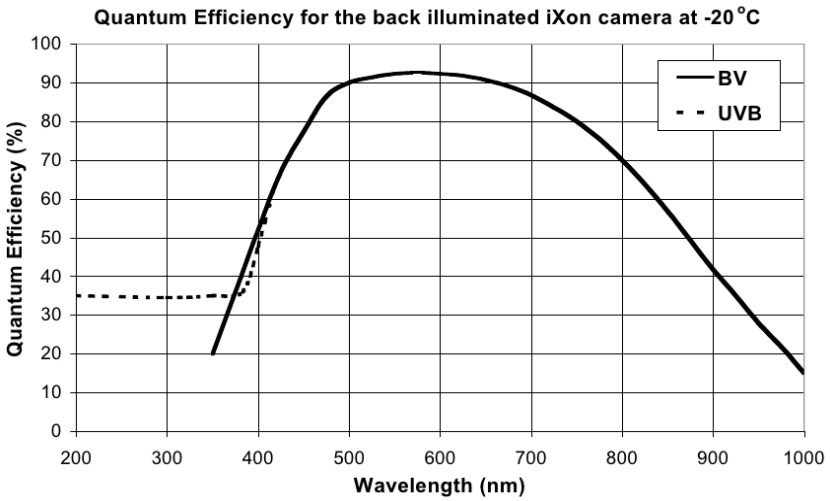

Figure 2: Quantum efficiency lies above 70% in the spectral range of the system.

2.3.3 Frame transfer CCD

The CCD in this camera is a so-called frame transfer device. Frame transfer CCDs use a two-part sensor in which one half of the parallel array is used as a storage region and is protected from incident light by a light-thight mask (see Figure 3). Light is allowed to fall on the uncovered part of the array and the

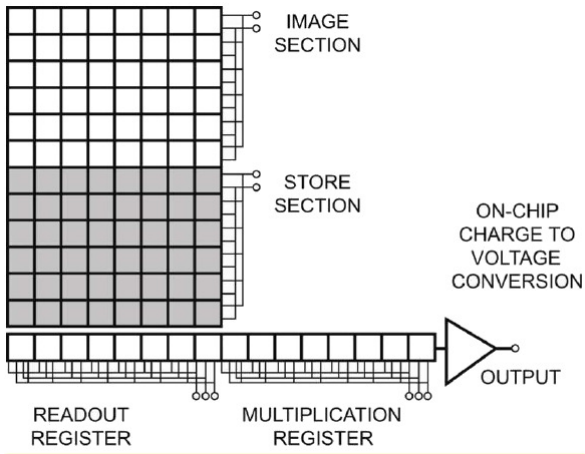

Figure 3: Frame transfer CCD

accumulated charge is rapidly shifted in to the storage region for charge transfer to the serial output register. While the signal is being integrated on the light-sensitive portion of the sensor, the stored charge is read out. The advantages of this mode of operation is that there is no need for a (slow) shutter — as the accumulated charge is rapidly shifted into the masked storage area — and higher frame rates compared to a conventional full frame CCD may be achieved on account of the high duty cycle. The minimum exposure time for a frame transfer CCD operated in frame transfer mode is the time taken to read out the image from the storage area. The steps in capture an image with a frame transfer CCD are given below.

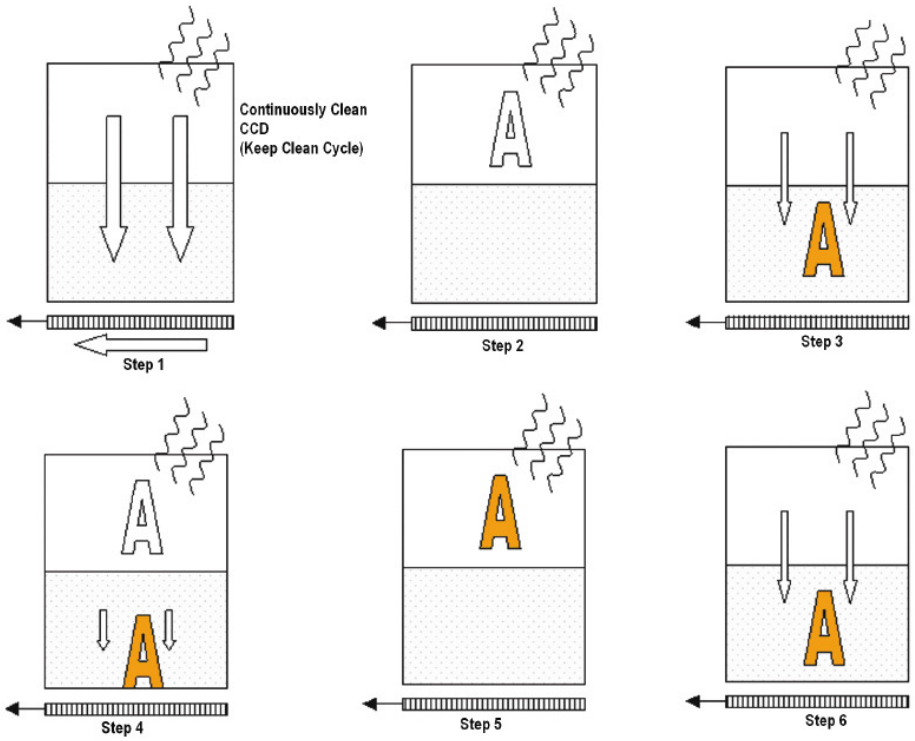

Figure 4: Capture sequence for a frame transfer CCD

Step 1: Both Image and Storage areas of the CCD are fully cleaned out, known as a Keep Clean Cycle.[1] Keep Clean Cycles occur continuously to ensure that the camera is always ready to start an acquisition when required.

Step 2: On receipt of a start acquisition command the CCD stops the Keep Clean Cycle. This allows the image (photoelectric charge) to build up in the Image area of the CCD. The CCD remains in this state until the exposure time has elapsed, at which point the readout process starts.

Step 3: The charge in the Image area is rapidly shifted into the Storage area. Once all the rows has been shifted, shifting in the Image area stops and

[1] The CCD is continually being read out, the accumulated charge is shifted out of the CCD.

charge begins to accumulate again, i.e. the next exposure starts.

Step 4: While the Image area is accumulating charge the Storage area is being read out.

Step 5: On completion of the readout, the system will wait until the exposure time has elapsed.

Step 6: The next cycle begins; repeat from Step 3.

As the captured image is quickly shifted into the storage section, a frame transfer CCD system can be used without a mechanical shutter. One potential drawback of this mode of operation is streaking of the image, as light is allowed to fall on the CCD while the image is shifted out. The streaking effect is alleviated by using a fast vertical shift speed in the CCD, thus minimizing the amount of light falling on the CCD during shifting.

2.3.4 Acquisition modes

The camera may be set up to capture images in different modes. Single Scan mode is self-explanatory; this mode does not allow for rapid acquisitions. To achieve high frame rates two modes may be used: Kinetic Series and Run Till Abort. In Kinetic Series mode a sequence of of single scans is captured into memory. Parameters that needs to be specified are the period between consecutive scans (Kinetic Cycle Time), exposure time, and total number of scans to be acquired (Figure 5). Run Till Abort mode is defined by the same parameters, except for total number of scans; acquisition does not end until the user aborts. The minimum possible delay between each scan will be the minimum Kinetic Cycle time. If the exposure time or the cycle time are set too low or are not permissible values, the driver will automatically calculate the nearest appropriate value not less than the input value. Note that frame transfer mode applies only to Kinetic Series and Run Till Abort modes.

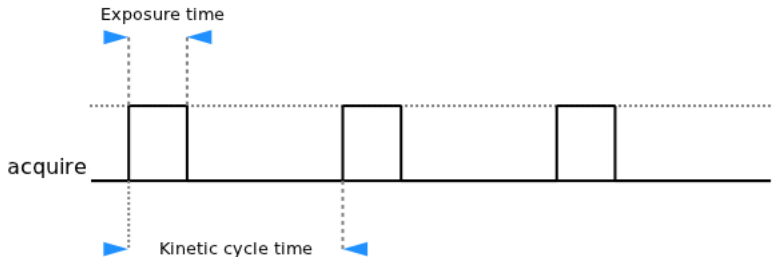

Figure 5: Kinetic Series mode

2.3.5 Frame rate and binning

The sensitivity and frame rate of the camera can be increased by a technique called binning. Binning allows charge from adjacent pixels to be combined, resulting in faster readout speeds and improved signal to noise ratios, albeit at the expense of reduced spatial resolution. Using binning means that the CCD in effect becomes more light sensitive because adjacent charges are combined. Both horizontal and vertical binning may be applied. Any increase in frame rate comes from vertical binning, but binning should be the same in each dimension so as not to distort the image data.

The EMCCD camera supports up to a 16×16 binning pattern, which reduces the image size to 32×32 pixels, and increases the frame rate to 167 frames per second. However, the increase in speed comes with a cost, and a compromise between frame rate and spatial resolution will have to be made. The disadvantage of binning, besides the obvious reduction in spatial resolution, is that objects will be harder to detect because the image data will become more noisy. A small object of interest may "drown" in the spectral data that are combined from the neighbouring pixels that are added together through the binning process. This effect gets worse the further the distance to the objects being imaged. For this reason binning should be kept quite low.

Tests carried out in the preliminary project shows what the actual frame rate of the camera is for different binning levels, summarized in Table 1. The camera

was configured with 1.8 µs vertical clock speed in full frame capture mode with different binning patterns. Series of frames was captured in Kinetic Series mode. Frame transfer mode was enabled and trigging was set to internal. Kinetic cycle time and exposure time was both set to 0, as this lets the driver calculate the fastest allowable timings. Cooling was off and gain was set to 1.

Binning	Max fps
1×1	17
2×2	32
4×4	61
8×8	107
16×16	167

Table 1: Camera frame rates

2.4 Acousto-optical tunable filter (AOTF)

A tunable filter is a device whose spectral transmission characteristics can be electronically controlled by applying a signal of some form; i.e. they are tunable band pass devices. An ideal tunable filter would have the attributes listed in Table 2 [5]. In practice these attributes are met only to a limited degree and different filter technologies offer different advantages and disadvantages.

AOTFs are based on the acousto-optic effect; the interaction between sound waves and light waves. By exciting a sound wave through a suitable crystal medium, light transmitted through the crystal is diffracted at a particular wavelength. To generate the acoustic wave, a radio frequency[2] (RF) signal is applied to a piezo-electric transducer attached to the crystal, causing it to vibrate. The acoustic wavelength is a function of the frequency of the RF signal; changing the frequency will change the wavelength of the diffracted light. As the acoustic waves pass through the crystal they cause the crystal lattice to be alternately compressed and relaxed. This results in periodic density changes in the crystal, changing the

[2] A frequency in the range of about 3 kHz to 300 GHz.

- Minimal tunability time
- Minimal out-of-band transmission
- Minimal physical thickness
- Low power consumption
- Polarization insensitive
- Selectable bandpass
- Minimal attenuation of light intensity
- Infinite spectral range
- Top-hat band pass curve
- Large aperture
- Constant bandpass
- Random access to wavelength
- Wide field of view
- Insensitive to environmental factors

Table 2: Ideal tunable filter attributes

index of refraction [10, 17]. The resultant refractive index variations act like a transmission grating or Bragg diffracter. Unlike a classical diffraction grating, however, the AOTF only diffracts one specific wavelength band of light, so that it acts more like a filter than a diffraction grating. This is a result of the fact that the diffraction takes place over an extended volume, not just at a surface or plane, and that the diffraction pattern is moving in real time [5].

The specific type of crystal medium used in the AOTF depends on the spectral range of interest. In AOTFs that operates from near the ultraviolet through the short wave infrared region (including the visible spectrum), a tellerium dioxide (TeO_2) or a Hg_2C_2 crystal is used, typically in a non-collinear configuration, meaning that the acoustic and optical waves propagates through the crystal at quite different angles. The operating principles of non-collinears AOTFs is illustrated in Figure 6.

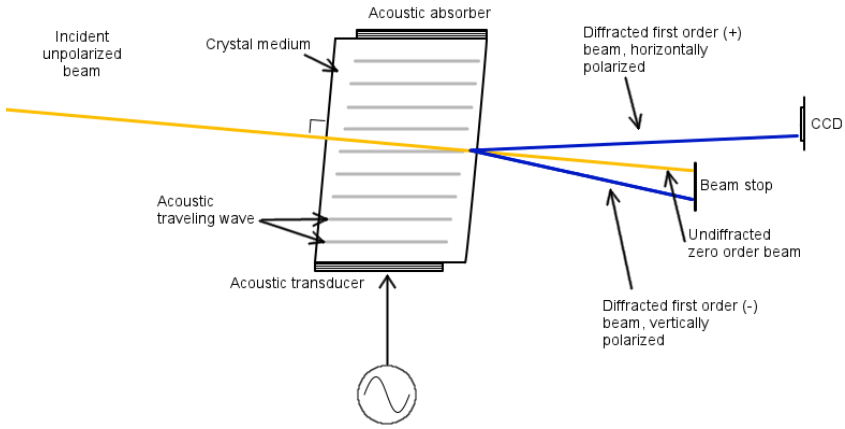

Figure 6: AOTF operating priciples

AOTFs can also be configured in a collinear fashion (for example, using quartz), where the incident light and the acoustic wave travel at the same angle through the crystal. The diffracted light is then also collinear with the input beam and acoustic wave. Because the polarization of the incident light beam is orthogonal to that of the diffracted beam, and the two beams are collinear, a polarizer must

be used to separate the beams [5].

In non-collinear AOTFs using tellerium dioxode crystals, the incident (zeroth order) and diffracted beams are physically separated and the filter does not require polarizers. Non-polarized incident light beams are diffracted into two orthogonally polarized first order beams, labeled the + and − beams (see Figure 6). The angle between the beams is dependent on device design, but typically ranges over just a few degrees [17]. In order to use a non-collinear AOTF as a tunable filter, the undiffracted (zeroth order) light beams needs to be blocked, allowing only the first order diffracted light to reach the camera sensor.

The accepted angle of incidence of the incoming light (field of view) on an AOTF is typically just a few degrees, requiring well-collimated[3] light to function properly. The tuning time for an AOTF is the time from a frequency change command is sent to the RF driver until the spectral output from the filter is stable. The time for the AOTF to stabilize at a new spectral band is roughly the propagation time of the acoustic wave through the crystal. The acoustic velocity of TeO_2 crystals is 620 $\frac{\mathrm{m}}{\mathrm{s}}$, resulting in tuning times in the order of tens of microseconds [18]. The time to switch the RF signal in the driver is much less than 1 µs, negligible compared to the propagation time of the acoustic wave. For example, a large aperture TeO_2 based AOTF with a height of 12 mm, like the one used in this project, results in a tuning time of $\frac{0.012\ \mathrm{m}}{620\ \frac{\mathrm{m}}{\mathrm{s}}} \approx 20$ µs.

The spectral output of the AOTF is controlled, as described above, by varying the frequency of the applied RF signal. The power of the RF signal is used to control the amplitude of the diffracted light, making it possible to compensate for varying efficiency of the camera at different wavelengths. Also, AOTFs allow multiple RF signals to be applied simultaneously. This enables us to select several spectral bands simultaneously, and — by controlling the power and the intervals between the RF frequencies — to adjust the passband shape, refer to Figure 7.

[3] Light whose rays are approximately parallel, dispersing minimally.

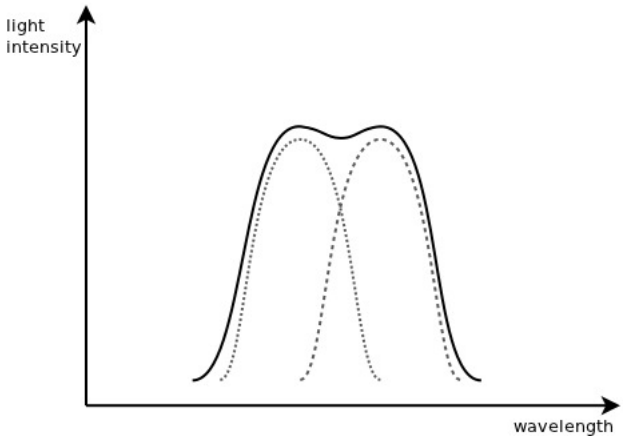

Figure 7: Combination of different spectral bands to change passband shape

2.5 Radio frequency driver

To drive the the AOTF a 16 channel radio frequency (RF) generator is used. The RF driver generates a RF signal with the frequency and power required to tune the AOTF. The signal synthesis is implemented by four, four channel Direct Digital Synthesizer (DDS) chips controlled by a master processor. Each channel is controlled individually. It has an USB interface for communicating with the host computer for control and setup. The driver has the ability to store in its own memory up to 64 complete sets of channel data, called profiles. A profile can be up to 16 channels. When loaded into the driver memory the RF driver will loop the saved profile set continuously. Alternatively, the driver may be initialized so that it will switch profile on each TTL pulse applied to its sync connector. The driver also have a TTL out signal that may be used to trigger a camera, with a configurable delay between changing profile and sending the trigger signal. There is also a immediate mode in which commands are processed as they are sent through the USB connection.

2.6 Optics

Because of the limited acceptance angle of the AOTF some consideration has to be given to limiting the angle of incidence of the incoming light on the face of the crystal. The AOTF will only diffract light that enters the crystal inside of the cone defined by the acceptance angle, centered on the optical axis.

The incident light needs to be collimated so it is approximately parallel to the optical axis before entering the AOTF. One solution is to use special collimating optical elements in front of the AOTF.Another solution is to configure the optics to be telecentric at some point before the filter [9].

2.6.1 Telecentricity

Telecentricity is the property of a multi-element lens design in which the principal rays are collimated and parallel to the optical axis in image and/or object space. Object space telecentric lens configurations have its entrance pupil at infinity and produces an orthographic view of the scene, having parallel principal rays in front of the lens system. Image space telecentric configurations have its exit pupil at infinity and parallel principal rays behind the lenses (at the sensor side). A simple way to make a lens telecentric is to put the aperture stop at one of the lens's focal points [19].

Conventional (entocentric) lenses exhibits parallax; close objects appear relatively larger than those placed farther away. This occurs because the principal rays in such systems are not all parallel to the optical axis. Telecentric lenses, on the other hand, produces an orthograpic view of the scene. In other words, telecentric lenses does not produce parallax; objects remain the same perceived size independent of their distance from the lens, over a range defined by the lens. This also means that the size of the largest object an (object side) telecentric system can capture is the same as the diameter if the lens [14].

The advantages of telecentric lens systems are:

- Reduction or elimination of perspective error (parallax).
- Reduction in distortion.
- Increase in image resolution.
- Uniform image plane illumination – An addition advantage of image space telecentricity is that it can lead to extremely uniform image plane illumination. The normal falloff in image plane illumination from the optical axis to the edge of the field is removed, since all principal rays are nearly perpendicular with respect to the image plane. Reflection onto neighbouring pixels and crosstalk between pixels are effectively eliminated.
- Constant magnification independent of shift in image and/or object planes.

2.7 LabVIEW

LabVIEW—developed by National Instruments—is short for Laboratory Virtual Instrumentation Engineering Workbench and is a platform and development environment for a visual programming language, sometimes referred to as G. LabVIEW is available for Microsoft Windows, UNIX, Linux and Mac OS X, and is commonly used for data acquisition, instrument control, industrial automation, signal analysis and processing, and embedded design. LabVIEW facilitates fast prototyping and easy data acquisition. G code is compiled, and may be targeted to other systems than the familiar desktop OS's. With the real-time extension module you may build applications for VxWorks or PharLaps ETS OS. There is also a FPGA module wich lets you target FPGAs directly. However, compiled executables buildt in LabVIEW are not truly standalone since they require the LabVIEW run-time engine to be installed on any computer that run the application. The run-time engine can be included in the build and shipped together with the application (requiring an additional licence for the application builder), it makes the application less portable than any written in more common languages that are supported by the major operating systems.

2.7.1 Dataflow programming

G is a dataflow programming language. In dataflow programming the focus is on *how things connect*; programs are modeled as a series of connections, with the operations between these connections being of secondary importance. Operations consist of blocks, that can be viewed as "black boxes" with inputs and outputs, all of which are explicitly defined. Whereas traditional programs essentially consist of a series of statements to be executed sequentially, dataflow programs let operations take place as soon as all the inputs of a block are available. Because of this, dataflow programs are inherently parallel. Actual parallel execution depend, of course, on the underlying hardware.

2.7.2 The G programming language

G programming is performed by wiring together graphical icons (or function nodes) on a block diagram, which is then compiled directly to machine code for execution. While represented graphically instead of textually, G contains the same programming concepts found in most other high-level languages. For example, G includes all the standard constructs, such as data types, loops, event handling, variables, recursion, and object-oriented programming, although the last two is quite new in G — native recursion was not supported until version 2009 and native object-oriented features until version 8.20 and does not necessarily feel quite like a integrated part of the language. With the implicit parallelism of a dataflow programming language, it is very easy to create parallel programs in G. That being the case, sections of code may often require sequential execution and care must be taken to ensure this, as well as to avoid race conditions — unintentional parallelism can have weird results. Fortunately, LabVIEW comes with a built-in debugger that allows the user to visually trace the dataflow and monitor variables. The built-in compiler continually works in the background to identify parallel sections of code. Whenever G code has a branch in a wire, or parallel nodes on the diagram, the compiler tries to execute the code in parallel within a set of threads that LabVIEW manages automatically.

Programs and subroutines in LabVIEW are called virtual instruments (VIs). Each VI is made up of three components: a block diagram, a front panel and a connector pane. The front panel is the user interface of the VI, and consists of controls and indicators that allows the user to input or view data from a running VI. The connector pane is used for representing the VI as a *subVI* in the block diagram of a calling VI. A subVI is analogous to a subroutine in other languages, and is a way of decompose a complex program into simpler modules. A VI can be run as a top-level program, with the front panel serving as the user interface, or as a subroutine when dropped as a node onto another blockdiagram, and defining the inputs and outputs for the node through the connector pane. If the application is targeted to a system without an UI, like an real-time target or FPGA, the front panel objects serves as local variables in the program.

3 AOTF-based spectral imaging system

In this section we present the system design and give some calibration procedures. The spectral imaging system consists of a digital camera with controller card, a host computer, an AOTF and a special optical layout that forms the images through the filter, and RF driver. The camera and filter are controlled from the host computer and have custom made software for image acquisition and processing. The optical layout are based on a design by Vila-Francés et al. [7]. A diagram depicting the system are shown in Figure 8.

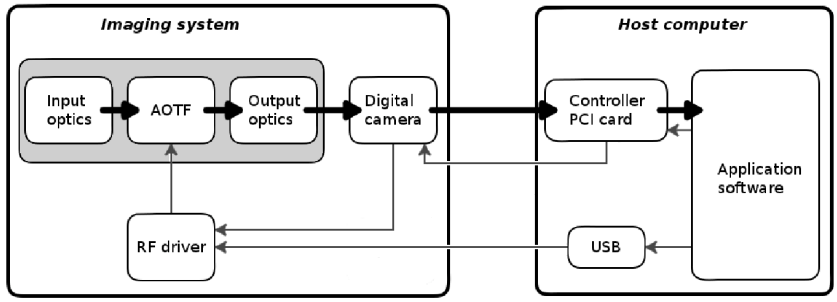

Figure 8: System overview diagram. Fat arrows signifies data flow, thin arrows signifies control flow.

3.1 Camera specifications

The camera interface with the computer through a dedicated PCI card, which has a frame grabber and microcontroller for acquiring image data and controlling the camera. An overview of the camera specifications is listed in Table 3.

3.2 AOTF specifications

We chose a TeO_2 based model from Gooch & Housego (model TF625-350-2-12-BR1A) with a wavelength range of 450–800nm, corresponding to drive frequencies

EMCCD camera specifications	
Active pixels	512×512
Pixel size	16×16 µm
Image area	8.2×8.2 mm
Max readout rate	5 MHz
Digitization	14 bit
Read noise (electrons)	< 1 to 45 @ 5 MHz (with electron multiplication)

Table 3: EMCCD camera specifications

of approximately 137–66MHz (see Figure 9c). The spectral range of the AOTF was chosen to best match the quantum efficiency[4] of the camera.

The properties of the AOTF are given in Table 4 and Figure 9 [20]. Note that all the values are calculated and is expected to vary a little from one device to another.

AOTF specifications	
Active aperture	11×12 mm
Transmission efficiency	$>$ 99.5%
Length of AO cell	41.5 mm (in optical direction)
Wavelength range	450 nm $< \lambda <$ 800 nm
Resolution (FWHM)	< 3 nm @ 500 nm($\Delta\lambda = 1.5$ nm typical) (refer to Figure 9a)
Side-lobe suppression	$>$ 30 dB (typical)
Beam separation	$\geq 4.5°$
RF drive power	< 0.5 W typical (wavelength dependent)
Maximun permitted drive power	5 W

Table 4: AOTF specifications

[4] Quantum efficiency is a measurement of the CCDs electrical sensitivity to light. It is measured over the spectral range of the CCD, giving the the efficiency at each photon energy.

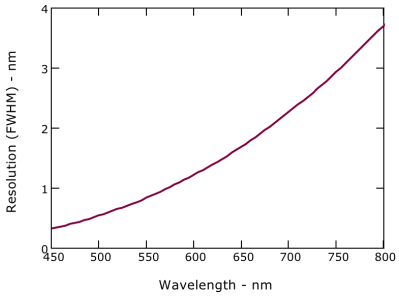

(a) Passband resolution

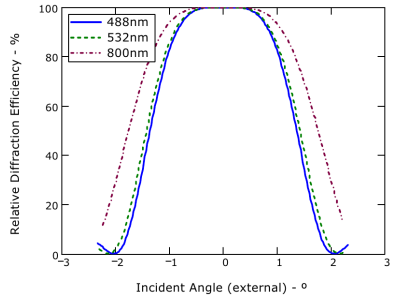

(b) Acceptance angle (external)

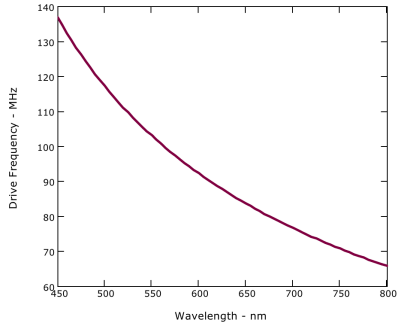

(c) Tuning relation

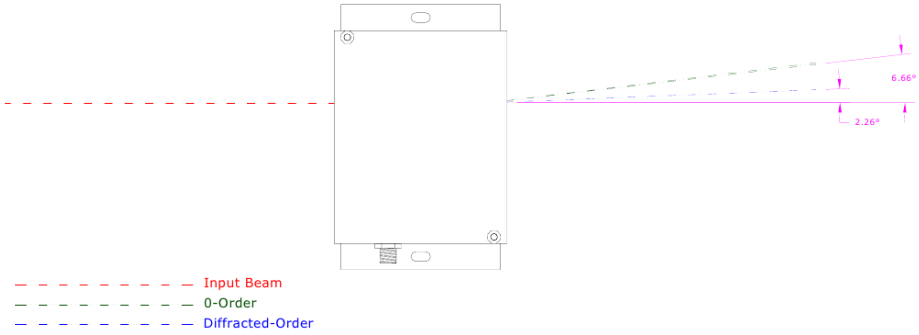

(d) Beam configuration

Figure 9: AOTF specifications

3.3 RF driver setup

The RF driver control software is written in LabVIEW. The USB interface for the RF driver uses an FTDI FT245R USB to RS232 converter. The controlling PC requires the driver software for this chip installed before the RF driver can be connected. It is available for download from the manufacturer's website: *http://www.ftdichip.com/Drivers/VCP.htm*

Connecting the RF driver
The RF unit is synchronized with the camera by connecting the "Fire" output of the camera to the "Camera In" connector on the driver housing, and using the internal trigging mode of the camera.

1. Connect the AOTF device to the RF driver.
2. Apply +24 V and +3.3 V to the RF driver as indicated on the driver housing.
3. Connect the RF driver to the PC with a USB 'A' to 'B' cable.
4. The first time this is done Windows will detect new hardware as a "USB serial port" and request a software driver. Select the "FTDIPORT.INF" file and install the driver.

The RF driver software is written in LabVIEW. In the "Device Type" selection, "CD7" should be selected. A frequency profile can now be saved in the RF driver and looped continuously, triggered by the camera "fire" pulses. In this way the RF driver is in standalone mode and does not require the host computer for operation.

3.4 Optical configuration

The optics of the system has been arranged so as to conform to the particular nature of the AOTF. As we have seen, the AOTF's restricted angular acceptance

requires well-collimated incident light. The solution we have chosen for this system is to make the optics telecentric before the filter [9].

The optic layout, shown in Figure 10, consists of a diaphragm and objective in front of the AOTF, making the system object side telecentric since the diaphragm is located at the focal plane of the objective. This restricts the angle of light entering the AOTF. After the AOTF another objective and diaphragm form the imaging optics, projecting the input image on the sensor plane. The optics are confocal with a common focal point between the input and the output lenses, inside the AOTF crystal. There are apertures at the object and image focal planes, and the system is therefore telecentric for both the object and the image space [19]. Crossed polarizers are introduced in order to cancel out the zero-order light [8].

When configuring the optics in this way the focused light will always have the same angular extent for all incident angles. This provides the AOTF with a constant input angular spread so that the resolution and efficiency of the AOTF, which are functions of the input angle, will be constant over the field of view of the imaged scene [9].

After interacting in the AOTF, the first order and zero-order diffracted beams are separated by the diffraction angle of the AOTF. The zero-order beam are blocked, while the first-order beam are projected through the output aperture.

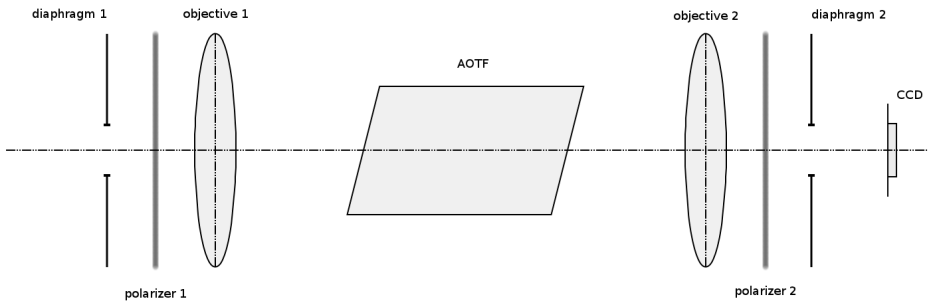

Figure 10: Schematic diagram of the telecentric confocal optics layout.

3.5 Application

The imaging system is controlled by a custom made application running on the host computer. The application is developed in LabVIEW and uses a software development kit (SDK) supplied by Andor for their camera range, which includes a LabVIEW software library and a win32 DLL. The control application that comes with the RF driver is also LabVIEW software.

The main application lets the user configure the relevant acquisition parameters via a graphical user interface, and start and stop the acquisition. There are two modes of operation, one which saves a series of image data to disk, and one which is made with online image processing in mind. The last one is made to utilize a multicore system, where one thread acquire the image data from the camera and another performs the image processing. In this way, the image processing algorithm may use a preallocated accumulation buffer for storing an intermediate result. This method is probably not useful for complete classification, but rather for target detection where the objective is to detect a certain spectral signature.

Image processing algorithms may be developed independently and dropped into the application as a submodule. LabVIEW has several options for image processing; a function node structure can be used for C like code implementation, or the MathScript RT node which supports a subset of Matlab m-file syntax. The application is documented in Appendix A.

3.6 Calibration

The imaging system and its use are not free from problems. Faults and nonlinearities in the sensor, aberrations in the optical subsystem, inhomogeneous illumination, limited spatial resolution of the sensor and limited resolution of the A/D converter all influence the results. A number of calibrations and corrections are necessary in order for the system to produce good quality images. The goal of calibration is to have the images as clean and accurate as possible to ease the subsequent image data analysis and give results that are easier to interpret.

The calibration of the system can be divided into several categories:

- *Radiometric calibration* – linking pixel intesities with a physical parameter.
- *Spectral calibration* – determining RF–wavelength tuning relation and spectral resolution.
- *Geometric calibration* – correcting optical aberrations.
- *Noise calibration* – correcting noise in the image acquision process.

3.6.1 Radiometric calibration

The A/D converter counts produced in the camera is in some arbitrary unit, defined by exposure time, camera gain, the quantum efficiency curve of the camera and intensity of the light source. For these data to convey meaning they must be linked to a physical quantity, such as % reflectance. This coversion is different for each wavelength band used and different for varying exposure times and gain used.

The combination of light source intensity, exposure time and EMCCD gain has to be adjusted to avoid saturation of the A/D converter. The gain should be set so that the peak A/D count value is about 75–90% of maximum for the most sensitive wavelength. A white, highly reflecting diffuse reflecting surface is a good test object for this [12].

3.6.2 Spectral calibration

The relation between the radio frequencies and the wavelength of the diffracted light output from the AOTF can be read from the datasheet of the AOTF (Figure 9c). This relation is already taken care of in the RF driver control application, the frequencies may be entered directly. If a more accurate tuning relation is needed it can also be found experimentally, but this requires special equipment [13]. The spectral resolution of the AOTF also varies with wavelength.

The bandwiths of the pass-bands may be widened by using several of the channels in the RF driver.

3.6.3 Geometric calibration

Using an AOTF in an imaging application means that the optical aberrations produced by the AOTF needs to be taken into consideration and corrected. Aberration occurs when light from one point of an object does not converge into a single point after transmission through the optical system. Aberrations leads to blurring of the formed images and need to be corrected when constructing the optical system or in software. The two most prominent AOTF aberrations, produced by dispersion during the diffraction process, are scene shifting (chromatic aberration) and blur [9, 21]. Chromatic aberration occurs when the AOTF is tuned; the refractive index of the TeO_2 changes with the frequency of the acoustic wave causing small variations in the angle of the diffracted beams, commonly known as scanning. This effect is compensated for in many AOTF designs by placing a prism wedge on the output face of the AOTF [22]. Blur, on the other hand, cannot be corrected in the same way. Using an AOTF with a relatively long interaction length will reduce the blur associated with the acousto-optic interaction [2]. Both blur and chromatic aberration may be corrected by using a configuring the optical elements in a telecentric configuration [9].

3.6.4 Noise calibration

As we have seen, the camera have several features that increase sensitivity and suppress noise. The EMCCD sensor amplifies the accumulated charge on the chip before shifting the charge into the shift register for readout. Together with back-illumination and cooling of the sensor head a higher signal-to-noise ratio is achieved compared to conventional CCDs. However, we will have a look at the main noise contributing factors and what steps can be taken to minimize noise in the acquired images.

The *detection limit* is a measure of the smallest signal that can be detected in a single readout. The smallest signal is defined as the signal whose level is equal to the noise accompanying that signal, i.e. a signal-to-noise ratio of unity. Sources of noise are:

- Shot noise of the signal itself (*photon noise*): The inter-arrival time of photons to the detector is not constant; in fact, photons arriving at the sensor can be described as a Poisson process. In a photo of an evenly illuminated surface, photon noise will show up as one pixel having a improperly lower value compared to its neighbours. This type of noise can not be removed since it is due to the stochastic nature of light.
- *Dark signal*: CCDs build up dark current whether the CCD is being exposed to light or not. Dark current is caused by thermally generated electrons that build up in the pixels of all CCDs. Dark current is not a significant problem for a cooled EMCCD. Using a short exposure time (less than a few seconds) and cooling the detector below 0°C will effectively remove most of the shot noise caused by dark current (dark signal).
- *Readout noise*: Noise from A/D convertion and amplification of the accumulated charge in the sensor.

If the signal is small, we can ignore its shot noise. Furthermore, if a suitably low operating temperature and short exposure time can be achieved, the lowest detection limit will equal the readout noise. As the gain is increased it will at some point begin to cause a decrease in dynamic range. To maintain as much dynamic range as possible it is advisable not to use a higher gain than is necessary to measure a signal. The amplifier will, even in scientific CCD, have a readout noise of a few electrons rms[5], increasing to tens of electrons rms at MHz readout rates. However, this noise will effectively be reduced by the multiplication factor of the gain register which, when high enough, will achieve noise levels below 1 electron rms.

In addition to these noise sources, variations in sensitivity across the sensor will

[5] Root mean square.

appear to add noise to the signal. This *fixed pattern noise* remain constant from read to read. The differences in electron count values between pixels are due in part to a variation in the dark signal produced by each pixel, and in part to small irregularities that arise during the fabrication of the CCD. Since fixed pattern noise is partly due to dark signal, it will change with temperature, but because it is fixed, it can be completely removed from a measurement by background substraction. Background substracting is done by taking a dark frame (no light hitting the sensor) and substracting it from subsequent light frames. Since dark current accumulates in the sensor over time, the exposure time of the dark frame must be the same as for the light frames. The dark and light frames should also have the same temperature, because dark current varies strongly with temperature. If the sub-exposure time for each spectral band is identical the same dark frame may be used for all frames. To get a more accurate noise calibration several dark frames may be taken. These dark frames are then "median combined"; the dark frames are combined, making a list of pixel values at each point in the array, then a master calibration frame is built by selecting the median value from the lists of pixels. This master dark frame is substracted from each frame in the acquisition.

4 Assembly and testing

In this section we give details of system assembly and testing. A summary of the system parameters is given in Table 5.

Parameter	**Value**
Wavelength range	450–800 nm
Interaction medium	TeO_2
Pixel size	16×16 µm
Field size	512×512 pixels
RF drive frequency range	65–135 MHz
Length of AO cell	41.5 mm (in optical direction)
Active aperture (AOTF)	11×12 mm
Polarisation (AOTF)	Linear – orthogonal to input
Lenses, 2 Schneider Xenoplan C-mount:	
Image circle	2/3" / 11 mm
Effective focal length	35 mm
Front focal length	6.5 mm
Back focal length	17 mm
F-number	1.9

Table 5: System parameters

4.1 Alignment of optics

Initially the system is assembled on an optical table. In order to ensure optimal diffraction efficiency the AOTF is aligned so that the face of the crystal is perpendicular to the optical axis. This alignment is done by aligning a laser on the optical axis and turning the AOTF until the back-reflected beam from the face of the crystal was parallel with the optical axis. The AOTF must be mounted on a rotating base with the face of the crystal in the center of rotation.

The front and back objective lenses are adjusted to form a telecentric confocal system, with aperture stops at the object focal planes of both lenses and a common focal point at the center of the AOTF crystal. Diaphragm apertures are placed at the front focal planes of both lenses (see Figure 10), and the opening of the apertures are adjusted so that the f-number matches the acceptance angle of the AOTF [9]. The acceptance angle of the AOTF is about 2° (see 9b). The f-number (n_f) of the two aperture–lens configurations is determined by the distance (f) from the aperture to the lens and the aperture diameter (d), thus $n_f = \frac{f}{d}$. Both apertures is adjusted to be the same distance from its lens and have the same diameter since both objective lenses are identical. The back lens is turned around and positioned with the back side towards the filter. The back focal plane of both lenses should be at the center of the AOTF crystal. The index of refraction of the TeO_2 affects the back focal length of the lenses, the new focal lenght becomes,

$$f_{\text{new}} \equiv a + b\, n_D$$

where a is the distance from the vertex of the last optical surface of the lens to the face of the crystal, and $b = f - a$ is the residual focal length inside the crystal (see Figure 11). The position of the lenses relative to the filter is calculated, setting the desired focal length to half the length of the crystal plus the displacement,

$$\begin{aligned} f_{\text{new}} &= \tfrac{l}{2} + a \\ a + b\, n_D &= \tfrac{l}{2} + a \\ (f - a)\, n_D &= \tfrac{l}{2} \\ a &= f - \tfrac{l}{2\, n_D} \end{aligned}$$

where f is the back focal length of the lens, n_D the refractive index of TeO_2 (measured at a wavelength of 589 nm) and l is the length of the AOTF crystal. With $f = 17$ mm, $n_D = 2.275$ and $l = 41.5$, we get $a = 7.9$ mm. This provides a guideline for the positioning of the lenses relative to the filter. During assembly of the optics the alignment is checked by visual inspection, simply looking in the

image side of the system. When the alignment is satisfacory, the crossed polarizer are placed in between the apertures and lenses (Figure 10.

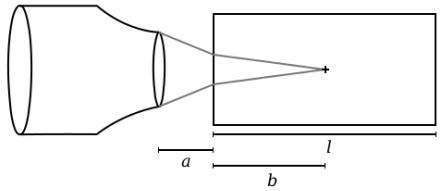

Figure 11: Positioning of the objective lenses relative to the AOTF.

After all the optics are in place the camera is added to the system. With the filter off, further alignment is made and checked by inspecting acquired images. When the alignment is satisfactory, some fine tuning is done to be sure the zero order light is blocked. Using a monochromatic laser and asserting that the beam is blocked when the filter is set to an arbitrary wavelength other than the laser wavelength. Conversely, when the filter pass band is tuned to the laser wavelenght we should see the laser in the acquired image. It is important that the laser is approximately parallel with the optical axis to ensure it is inside the acceptance angle.

4.2 Synchronization

The issue of synchronization of the camera and AOTF has been solved in the preliminary project, where we showed that the synchronization could be solved by using a signal pulse that the camera sends out at the start of each acquisition cycle. The reason for this is that the at the start of an acquisition cycle the camera rapidly shifts out the image acquired in the previous cycle into the storage area of the CCD. And during this time period the filter should change its pass-band since the camera is not exposing. The camera has to shift 512 lines at the start of each cycle regardless of any binning applied, and assuming we are using the fastest vertical clock speed of 1.8 µs, the filter need to stabilize inside a time

Spectral bands	
Central wavelength [nm]	Approximate resolution (FWHM) [nm]
450	0.3
490	0.4
530	0.5
570	1.0
610	1.2
650	1.5
690	2.0
730	2.3
770	3.0
800	3.5

Table 6: Spectral bands used during testing.

interval of $512 * 1.8 \approx 920\,\mu s$. This tuning time of the filter is, as shown in section 2.4, about $20\,\mu s$ giving a huge margin.

The camera is connected to the RF driver unit with a $50\,\Omega$ coax cable: The "Fire" SMB connector of the camera is connected to the "Camera In" SMA connector on the RF driver unit. A sheet of paper printed with different colors is used as the subject. The RF driver is loaded with a set of 10 spectral profiles, each specifying one channel, spread evenly over the spectral range of the AOTF, as shown in Table 6. The driver loops through the profile set, tuning the spectral band-pass of the AOTF each time the fire signal is received by the RF unit. The camera is set to capture series of 10 frames at a time which is inspected after the acquisition. The exposure time and gain is tuned experimentally until the image data is acceptable. The monochrome images should show different intensity for each colour over the range of images.

5 Discussion

5.1 Quality of the design

When assessing the qualities of the system described in this report it is natural to compare it with other types of spectral imaging systems, particularly push-broom systems. Push-broom imagers use a diffraction grating or a prism to to acquire many hundreds of wavelength data points simultaneously, while acquiring the field of view sequentially. Our system, being a tunable filter spectral imager, acquire wavelengths sequentially. This places one important restriction on the system: There should be minimal relative movement between the subject and the imaging system during acquisition. Even with very fast image acquisition rates, the system needs to be nearly stationary in order to avoid spectral blurring. The tolerance for movement depend, of course, on the application; the size and distance of the subject under inspection. This may not be an issue for a laboratory prototype such as this which is not very portable. But bearing in mind the long-term goal of making a portable spectral imaging system which relays real-time spectral or chemical video to the user, the frame rate have to be increased. If the imager is to be a handheld system the frame rate needs to be high enough that small movements does not introduce too much spectral blurring. Even with small movements the ability of the system detect small objects decreases. To increase accuracy of detection in a portable system it should probably be mounted on a tripod.

The main challenge in developing a high speed spectral imaging system is getting sufficient amount of light onto the the sample, and efficiently collecting the light reflected or transmitted by the sample. The light collection efficiency of a spectral imager depend on its light througput, optical transmission and polarization characteristics. The light throughput of this system is limited by the small field of view of the AOTF. Even though the filter has high transmission efficiency it requires linearly polarized incident light in order to work properly and need a linear polarizer in front of the input side. With randomly polarized incident light

this results in 50% loss. Losses due to optical transmission is kept as low as possible by using good quality objective lenses with high f-numbers. The light needs to be collimated to be relayed through the AOTF, which has a relatively long interaction length. To do this we chose to make a telecentric optical system. The telecentric layout corrects the aberrations in the AOTF, but severely limits the field of view. The field of view would be somewhat larger if an AOTF with a shorter interaction length was used. There is a tradeoff between diffraction efficiency and field of view, shorter AOTF need more power to diffract the light and have stronger aberrations.

The high configurability of the AOTF also makes the calibration of the system complex. Constant spectral resolution is a desired property of a spectral imager. Since the band-pass of the AOTF is not constant for different wavelengths it has to be configured to vary the band-pass over the spectral range. After deciding on the central wavelengths to be used in the specific application the band-pass has to be configured by utilizing several of the RF driver channels to compose a new band-pass shape. In addition, since the camera does not allow for variable integration time during an acquisition series, compensation for the varying quantum efficiency of the camera will have to be done by changing the band-pass in the filter or by scaling in software.

5.2 Implications

The image readout speed of the system determine if it is suitable for real-time spectral imaging. In our case it is clear that speed is a severe limitation in this regard.

Used as a hyperspectral imaging system using upwards of 50 spectral bands[6], the system is clearly not capable of real-time video. As an example, using 50 spectal bands and the shortest available exposure time of the camera, the time taken to acquire full image cubes is as shown in Table 7. As explained in section 2.3.5 the

[6] There is no clear limit on the number of spectral bands that makes up a hyperspectral imager, but from tens to several hundreds are not uncommon.

amount of binning should be kept low as not to hamper target discrimination by reducing the spatial resolution of the imager.

Binning	Spatial resolution [pixels]	Frame rate (single) [fps]	Snapshot time (image cube) [ms]
1×1	512×512	17	2941
2×2	256×256	32	1563
4×4	128×128	61	820
8×8	64×64	107	467

Table 7: Time to acquire a hyperspectral image cube using 50 spectral bands.

The current design is able to acquire at a rate of 32 frames per second, using a 2×2 binning pattern for an acceptable spatial resolution of 265×256 pixels. Clearly the time taken to acquire a hyperspectral data cube is in the range of several seconds, assuming there is enough light reaching the sensor so that the readout rate is the limiting factor. To speed up the image rate the number of wavelength data points to acquire may be limited, essentially making the system multispectral. The selection of which set of spectral bands to use depends on which substance the user are trying to detect, and will have to be configured anew for each target substance in general.

Comparing this system to a push-broom imager, the advantages are not very clear. Even though the camera can be replaced by one with better specifications, the light collection efficiency of the system is not very high. Push-broom imagers require line illuminationm while AOTF imagers require uniform illumination over a larger area, which is much harder to achieve. Furthermore, by only illuminating a narrow strip the push-broom imager can provide higher intensity with the same total light source power as the AOTF imager. More light means shorter exposure times and higher image rates.

5.3 Suggestions

In order to increase the frame rate of the system a faster camera could be used. There are newer EMCCD cameras [23] that operates at 56 frames per second at full frame (512×512 pixels), or 595 frames per second at 128×128 pixel image size. Features such as USB 2.0 interface with universal "plug-and-play" functionality ease the integration with a host computer. This would allowing the use of laptops or other small footprint systems and real-time operating systems without the need to port a driver. Cameras with CMOS sensors offers even greater speed at higher resolutions due to parallel addressing of pixels and on-chip signal processing [11]. However, care must be taken when considering CMOS technology in that they use rolling shutters which may cause undesired effects in high speed applications. There exists hybrid CCD/CMOS sensor, under the name "sCMOS", that emulates the exposure sequence of a CCD, allowing for "snapshot imaging", whereby all pixels begin the exposure simultaneously and end the exposure simultaneously, ensuring time-correlated capture.

6 Conclusion

The purpose of this study has been to design a spectral imaging system consisting of a digital camera with an acousto-optic tunable filter as the wavelength selective element, and evaluate the system's capacity for real-time spectral video. The challenges of incorporating the AOTF in an imaging system have been examined, and necessary calibration procedures have been given. This has resulted in a telecentric confocal optics design, which minimize aberrations produced by the AOTF. We have also assessed the strengths and weaknesses of AOTF spectral imagers versus push-broom spectral imagers. We have given a overall design of the imaging system, considering the many system integration considerations that is needed, and custom software have been developed. The premise for this project was form the basis for a chemical imaging system which could perform chemical identification and quantification in real-time, displaying the results in a video overlay of the imaged scene.

The spectral imaging system presented is able to funtion as a hyperspectral imager, the drawback being that the image rate is to low for real-time spectral video using more than a few spectral bands. The imager have configurable spectral selectivity making it more flexible than traditional spectral imagers, and can be configured according to the specific application. In this way the frame rate may be increased compared with full hyperspectral acquisition, but it requires complete knowledge of the spectral characteristics of the target material.

Another concern of the imager is the low light collection efficiency. It requires strong, even illumination over the whole field of view. The camera have good light sensitivity, but rather poor spatial resolution further limiting the usefulness when imaging a larger area. Furthermore, the requirement of a full size PCI-card for data acquisition and external power-supply for cooling of the camera head makes for poor mobility. The proprietary PCI-card also means that the choice of operating system is limited to Windows. This impedes the real-time capability of image processing and spectral video.

There is no significant advantage of using a AOTF based hyperspectral imager

over a push-broom system when it come to acquisition speed. The main strenght of the system is the flexibility offered by the AOTF in selecting certain wavelengths and varying the band-pass, and is therefore not ideal for hyperspectral imaging. This system is not capable of producing real-time hyperspectral images.

References

[1] J. Dubois, J. C. Wolff, J. K. Warrack, J. Schoppelrei, and E. N. Lewis. NIR chemical imaging for counterfeit pharmaceutical product analysis. Web, February 2007. URL `http://spectroscopyonline.findanalytichem.com/spectroscopy/article/articleDetail.jsp?id=406629`. Retrieved 13 December 2011.

[2] J. Ward, M. Farries, C. Pannell, and E. Wachman. An acousto-optic based hyperspectral imaging camera for security and defence applications. In *Proc. SPIE 78350*, 2010. doi: 10.1117/12.864972.

[3] C. Xie. Visualizing chemistry with infrared imaging. *J. Chem. Educ.*, 88(7): 881–885, March 2011. doi: 10.1021/ed1009656.

[4] M. Spring, C. Ricci, D. Peggie, and S. G. Kazarian. FTIR imaging for the analysis of organic materials in paint cross sections: case studies on samples from paintings in the National Gallery, London. *Anal. Bioanal. Chem*, 392: 37–45, 2008.

[5] N. Gat. Imaging spectroscopy using tunable filters: a review. In *Proc. SPIE*, volume 4056, pages 50–64, 2000.

[6] R.B. Smith. Introduction to hyperspectral imaging with TNTmips. Web, July 2006. URL `http://www.microimages.com/getstart/hyprspec.htm`. Retrieved 3 Nov. 2011.

[7] J. Vila-Francés, J. Calpe-Maravilla, L. Gómez-Chova, and J. Amorós-López. Design of a configurable multispectral imaging system based on an AOTF. *IEEE Transactions on Ultrasonics, Ferroelectrics and Frequency Control*, 58 (1):259–262, January 2011. ISSN 0885-3010. doi: 10.1109/TUFFC.2011.1795.

[8] J. Vila-Francés, J. Calpe-Maravilla, J. Muñoz-Mari, L. Gómez-Chova, J. Amorós-López, E. Ribes-Gómez, and V. Durán-Bosch. Configurable-bandwidth imaging spectrometer based on an acousto-optic tunable filter.

Review of Scientific Instruments, 77:073108, 2006. ISSN 00346748. doi: 10.1063/1.2221542.

[9] D.R. Suhre, L.J. Denes, and N. Gupta. Telecentric confocal optics for aberration correction of Acousto-Optic tunable filters. *Applied Optics*, 43 (6):1255–1260, February 2004. doi: 10.1364/AO.43.001255.

[10] N. Gupta. Hyperspectral imaging using acousto-optic tunable filters. In *Proc. SPIE 3718*, volume 3718, pages 512–521. SPIE, 1999. doi: 10.1117/12.359988.

[11] M. Farries, J. Ward, A. Killey, P. Dale, and A.S. Blagg. A high speed spectral imaging camera with the potential for Real-Time spectral video imaging. Gooch & Housego. Web, 2011.

[12] P. Geladi, J. Burger, and T. Lestander. Hyperspectral imaging: calibration problems and solutions. *Chemometrics and Intelligent Laboratory Systems*, 72(2):209–217, 2004.

[13] J. Liu, Y. Ma, L. Zhang, J. Wang, and R. Shu. Calibration of an AOTF hyperspectral imager with configurable spectral selectivity. In *Proc. SPIE 8196*, pages 819623–819623–10, 2011. doi: 10.1117/12.902306.

[14] M. Sonka, H. Vaclav, and R. Boyle. *Image Processing, Analysis, and Machine Vision*. Cengage Learning, third edition, 2008. ISBN 978-0-495-24438-7. International Student Edition.

[15] C.I. Chang. *Hyperspectral imaging: Techniques for spectral detection and classification*, volume 1. Springer US, 2003.

[16] N. Gat, G. Scriven, J. Garman, M. D Li, and J. Zhang. Development of four-dimensional imaging spectrometers (4D-IS). In *Proc. SPIE*, volume 6302, page 63020M, 2006.

[17] D.J. Brady. *Optical Imaging and Spectroscopy*. Wiley, Hoboken, NJ, USA, 2009. ISBN 9780470443729.

[18] N. Menn. *Practical optics*, chapter 7, pages 234–250. Elsevier Academic Press, Amsterdam, 2004. ISBN 0-12-490951-5.

[19] M. Born and E. Wolf. *Principles of Optics*. Pergamon, New York, 6 edition, 1980.

[20] TF625 Manual. *TF625-350-2-12-BR1A*. Gooch & Housego, June 2010.

[21] D. R. Suhre, M. Gottlieb, and N. T. Nelamed. Spatial resolution of imaging noncollinear acousto-optic tunable filters. *Opt. Eng.*, 31(10):2118–2121, 1992. doi: 10.1117/12.58882.

[22] T. Yano and A. Watanabe. Acoustooptic TeO_2 tunable filter using far-off-axis anistropic Bragg diffraction. *Appl. Opt.*, 15(9):2250–2258, 1976. doi: 10.1364/AO.15.002250.

[23] Andor Technology. Web. URL `www.andor.com`. Retrieved 22 May 2012.

Appendices

A LabVIEW diagrams

Listed in this section are the LabVIEW diagrams for the camera control and acquisition application are included, in the following order:

1. Top level VI.
2. Parameter setting VI.
3. Multicore acquisition VI.
4. Singlecore acquisition VI.
5. Temperature control VI.
6. FPS calulating VI.
7. Error handler VI.
8. Camera shutdown VI.

Note that the subVIs developed for this project can be recognized as the green blocks in the diagrams. The purple ones are from the Andor SDK. In case of multiple stacked subdiagrams, as in case structures, the different subdiagrams are listed below the main block diagram.

Connector Pane

iXonDV887.vi

Top level VI for the iXon camera application. Set the camera parameters, the driver reports the actual values.
Pressing Start Acquisition brings up the acquisition window.
The number of accumulation is for illustrating image processing, this number of frames will be added to form one image to display.

Front Panel

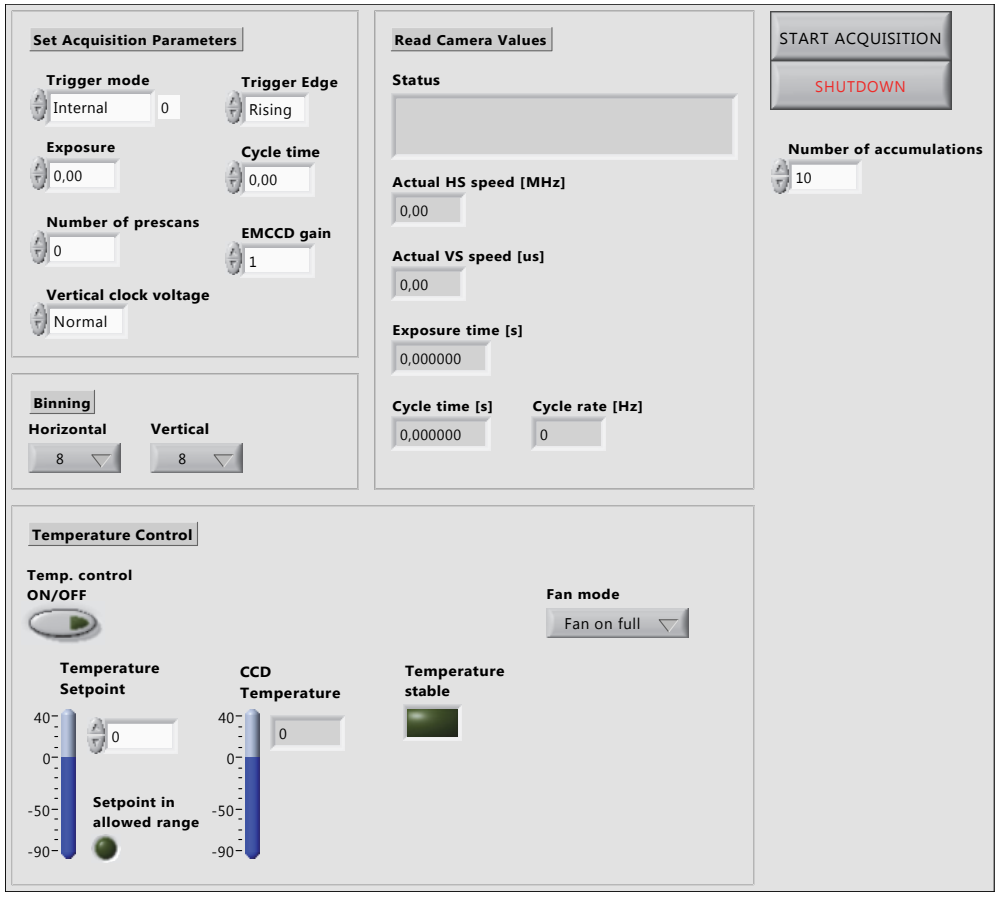

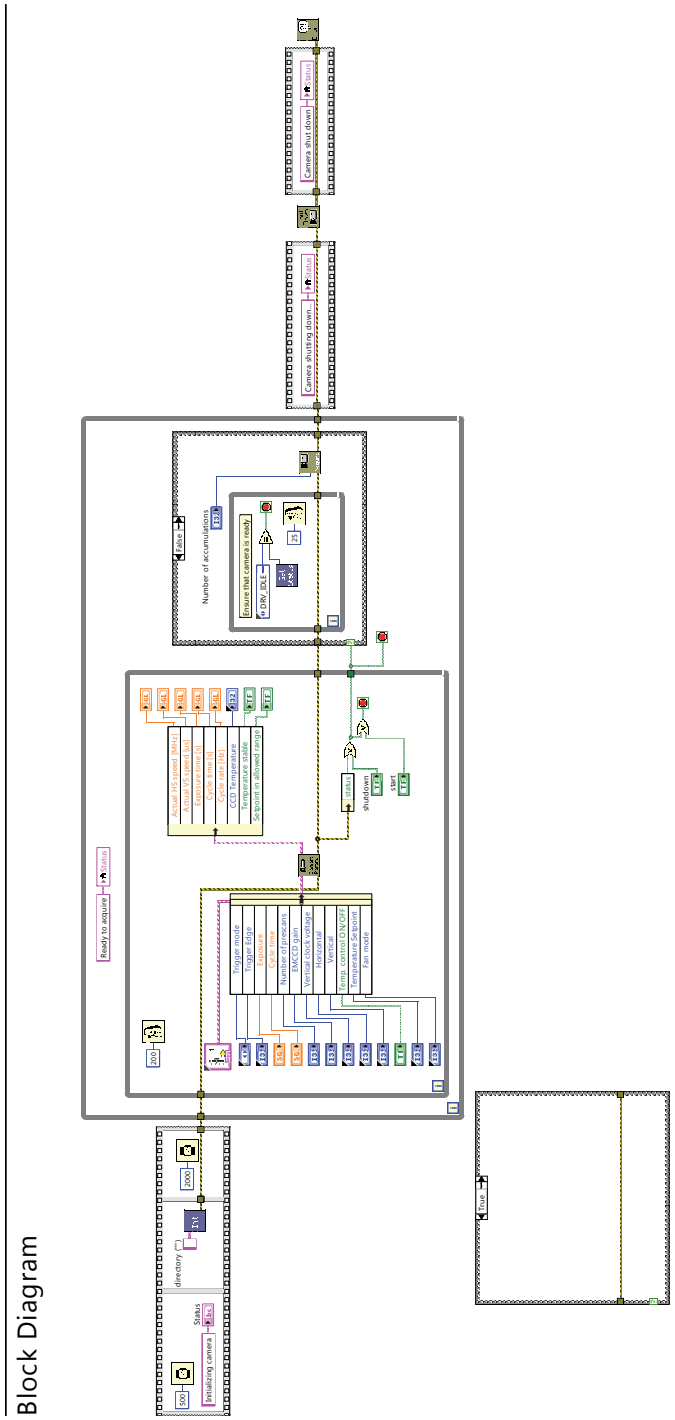
Block Diagram
Camera shut down
status
Camera shutting down
status
Number of accumulations
Ensure that camera is ready
DRV_IDLE
Actual H.S speed (MHz)
Actual V.S speed (µs)
Exposure time (s)
Cycle time (s)
CCD temperature
Temperature status
Setpoint in allowed range
Ready to acquire
status
shutdown
start
Trigger mode
Trigger Edge
Exposure
Acquire mode
Number of precasts
EMCCD gain
Vertical clock voltage
Horizontal
Vertical
Temperature Setpoint
Fan mode
200
directory
Status
Initializing camera
100
true

Connector Pane

SetParameters.vi

Control cluster — output cluster

error in (no error) — error out

Block Diagram

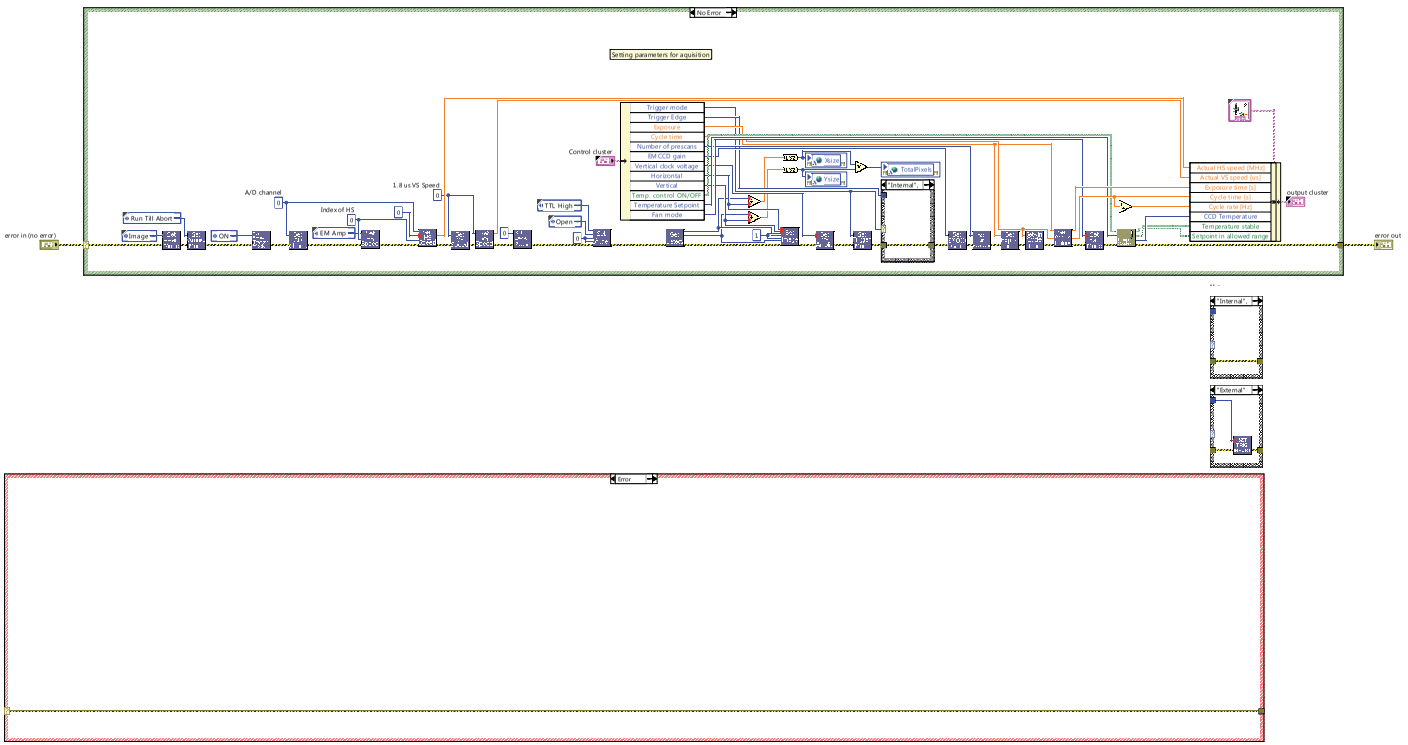

Connector Pane

Acquire_multicore.vi

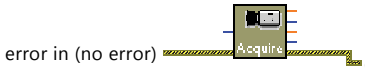

Image acquisition suitable for multicore systems.
A producer/consumer design: The producer loop acquires each image when an interrupt from the camera occurs. The consumer loop processes each frame in parallel, synchronized by a queue. Individual frames are added together up to the set number of accumulations, and then displayed on the front panel.

Front Panel

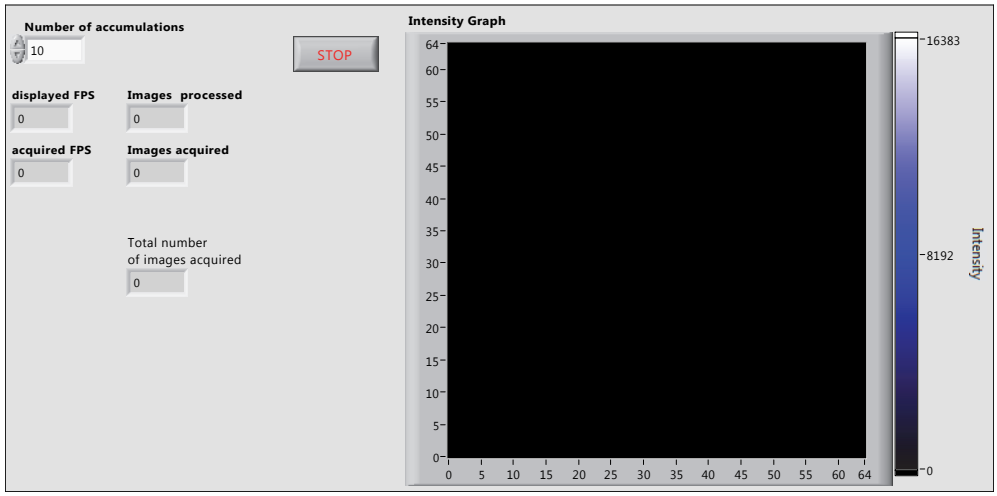

Block Diagram

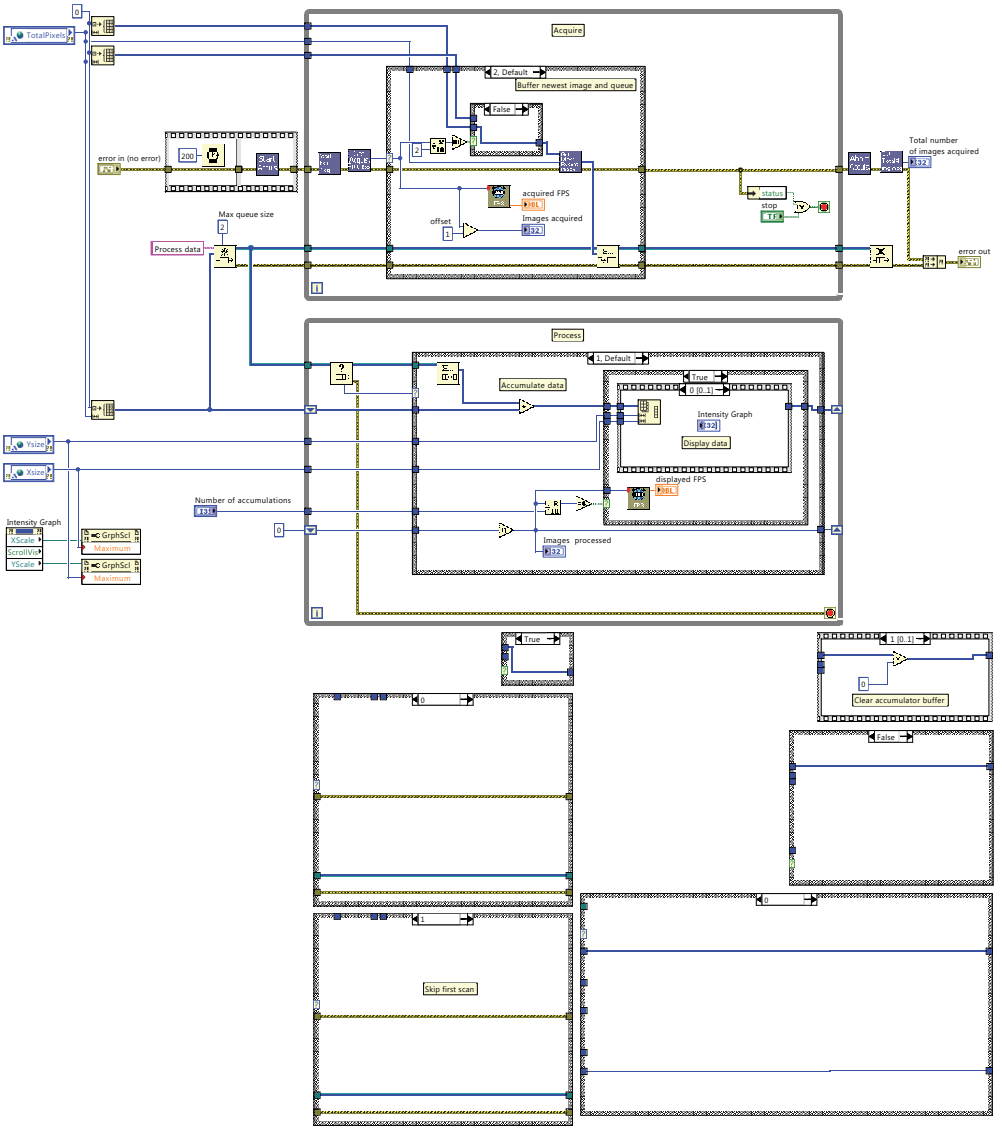

Connector Pane

Acquire_singlecore.vi

error in (no error) error out

Image acquisition suitable for singlecore system. Both processing and acquisition is done in the same loop. Individual frames are added together up to the set number of accumulations, and displayed on the pront panel.

Front Panel

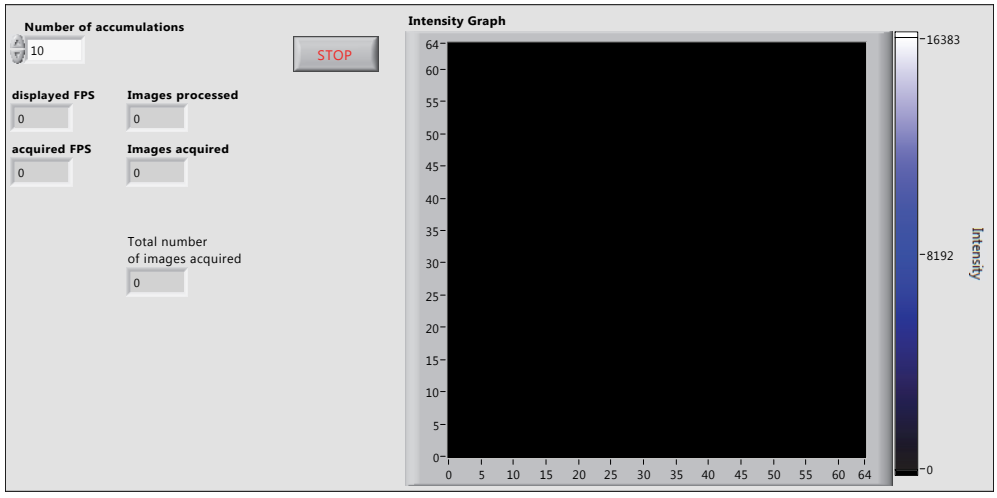

Block Diagram

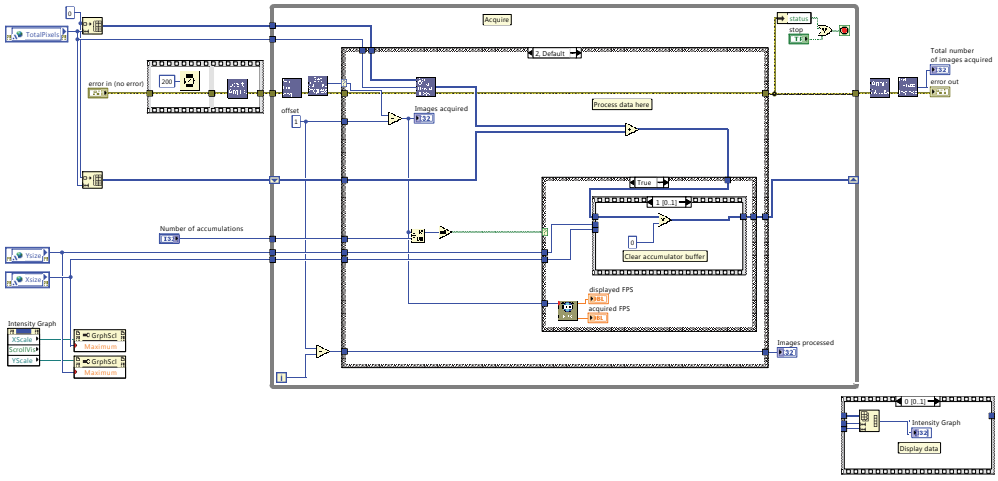

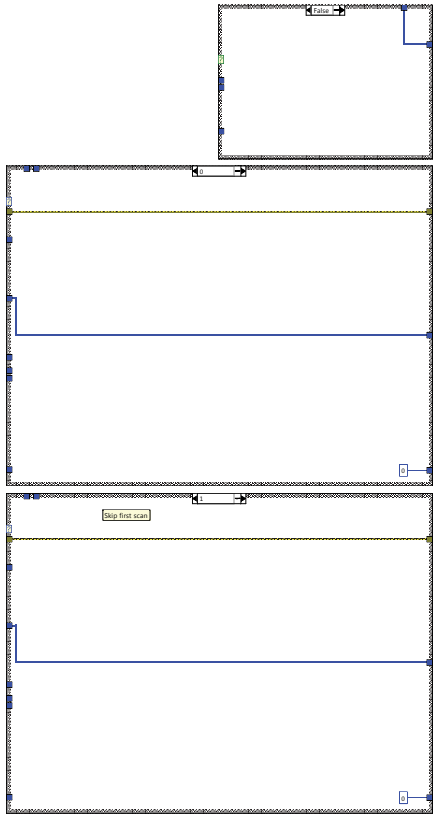
False
0
0
1
Skip first scan
0

Connector Pane

TemperatureControl.vi

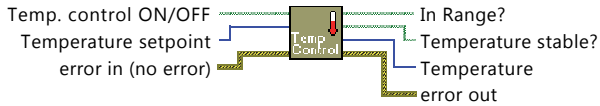

Block Diagram

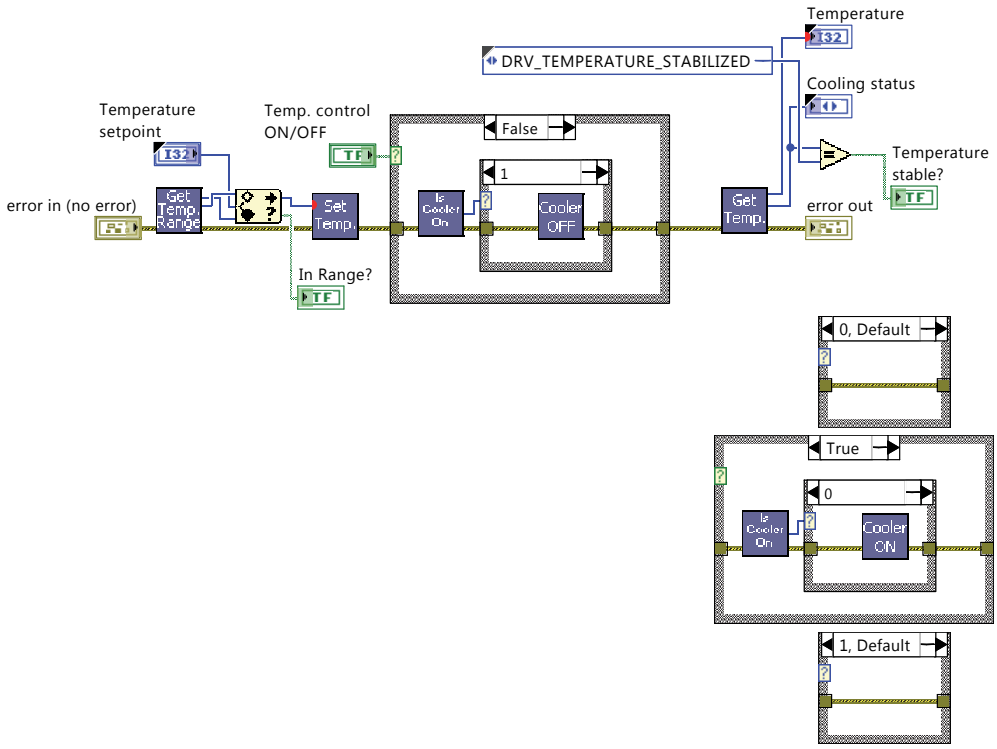

Connector Pane

CalculateFPS.vi

frame number

Block Diagram

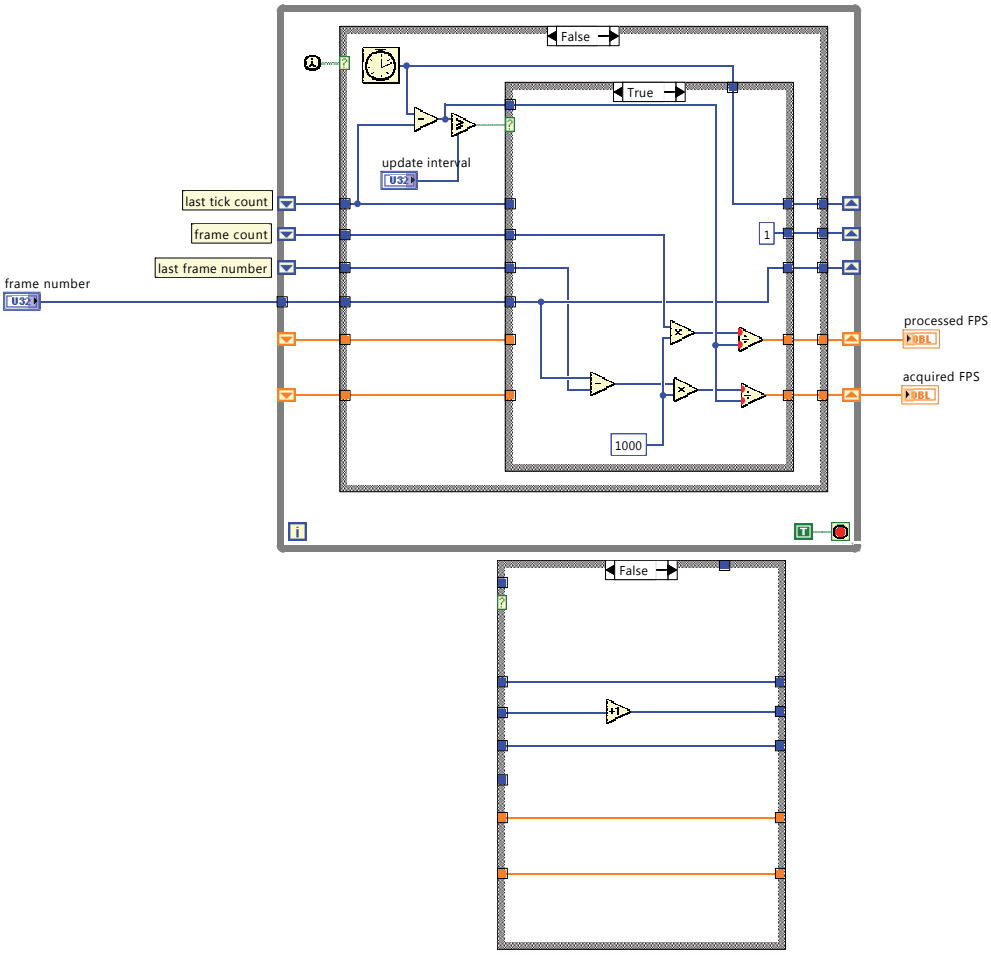

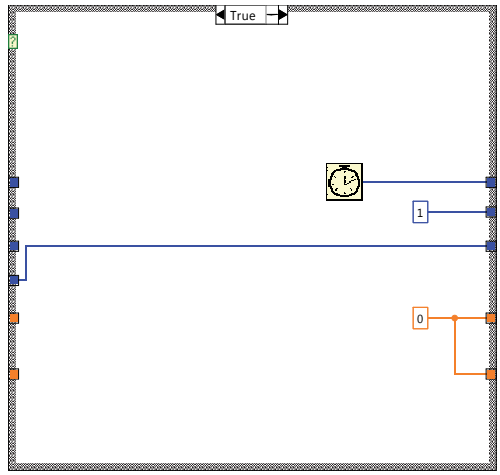
True
1
0

Connector Pane

CamErrorHandler.vi

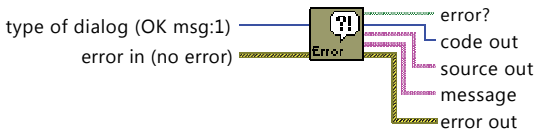

Block Diagram

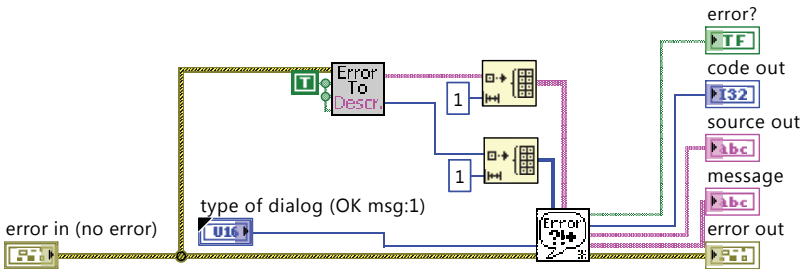

Connector Pane

ShutdownCamera.vi

Block Diagram